IEEE Access
Multidisciplinary | Rapid Review | Open Access Journal

Received 6 September 2023, accepted 15 September 2023, date of publication 4 October 2023, date of current version 11 October 2023.

Digital Object Identifier 10.1109/ACCESS.2023.3321692

RESEARCH ARTICLE

Robust Real-Time Shipboard Energy Management System With Improved Adaptive Model Predictive Control

WENJIE CHEN[1,2], (Member, IEEE), KANG TAI[2], MICHAEL WAI SHING LAU[3], (Life Member, IEEE), AHMED ABDELHAKIM[4], (Senior Member, IEEE), RICKY R. CHAN[5], ALF KÅRE ÅDNANES[6], AND TEGOEH TJAHJOWIDODO[7]

[1]ABB Pte. Ltd., Singapore 139935
[2]School of Mechanical and Aerospace Engineering, Nanyang Technological University, Singapore 639798
[3]School of Mechanical and Systems Engineering, Newcastle University in Singapore, Singapore 567739
[4]Epiroc Rock Drills AB, 70191 Orebro, Sweden
[5]ABB Group (Marine & Ports), 00980 Helsinki, Finland
[6]ABB Group (Marine & Ports), Shanghai 201319, China
[7]Department of Mechanical Engineering, KU Leuven, De Nayer Campus, 2860 Sint-Katelijne-Waver, Belgium

Corresponding authors: Wenjie Chen (jessie.chen@sg.abb.com) and Kang Tai (mktai@ntu.edu.sg)

This work was supported in part by Singapore Economic Development Board-ABB Pte. Ltd., Joint Industrial Postgraduate Program.

ABSTRACT The electrified hybrid shipboard power system with high-level integration of renewable energy resources and energy storage system has become the new trend for the all-electric ship (AES) configuration. However, the traditional rule-based energy management system (EMS) is not able to fulfill the increasingly complex control requirements, and a more advanced EMS control algorithm is required to handle the multiple power sources and even achieve optimal energy management control. This paper proposes a supervisory-level EMS with an improved adaptive model predictive control (AMPC) strategy to optimize the power split among the hybrid power sources and to reduce the total cost of ownership (TCO) of vessel operation, which considers not only the fuel and emission costs but also the power source degradation. In order to achieve real-time implementation, the AMPC-based EMS software has been developed and deployed to a programmable logic controller (PLC) hardware. The prototyping controller verification tests have been performed with a hybrid fuel cell-fed shipboard power system hardware-in-the-loop (HIL) plant in the lab environment. Three typical tugboat load profiles with power fluctuations are implemented as case studies. Lastly, a cost study was performed to compute the economic benefits for a ten-year long-term vessel operational cycle. The proposed AMPC-based EMS is robust and effective, which can achieve up to 12.19% TCO savings compared to those of a traditional rule-based control strategy.

INDEX TERMS All-electric ship, hybrid shipboard power microgrid, adaptive model predictive control, energy management control system.

I. INTRODUCTION

With increasingly strict environmental rules and regulations [1], [2], the all-electric ship becomes one of the most promising solutions to comply with these new requirements. The DC-grid shipboard power system has shown its advantage of higher efficiency in power distribution and allows for more flexible designs and modes of operation that simplify the integration of different types of renewable power sources, such as fuel cells and batteries. However, this type of hybrid power integration has greatly increased the complexity of the power system and control requirements [3]. The energy management system (EMS), the essential control system for marine vessel operation, is the brain of a shipboard power system to handle different aspects of vessel operations. The traditional EMS, usually with a rule-based control strategy,

The associate editor coordinating the review of this manuscript and approving it for publication was Zheng Chen.

has limitations in managing the multiple power devices operation, as well as considering fuel efficiency, reducing emissions and extending the device lifetime. An advanced energy management control algorithm is required to handle the increasing complexity of the power system under different operation modes, and also to achieve optimal control.

A hierarchical control scheme has been widely accepted as an industrial standard for shipboard EMS [4]. In this multilevel control framework, the primary and secondary control levels handle the instantaneous load sharing among the hybrid power devices and system local coordination, which has been explored in the authors' earlier research work [5]. In this study, a tertiary-level EMS is proposed to optimize the power allocation for hybrid power devices and minimize the total cost of ownership (TCO) for a shipboard power system.

According to optimization theory, tertiary-level energy control can be classified as rule-based or optimization-based EMS [6]. The researchers presented in-depth reviews of marine energy management systems [7], [8], [9]. Rule-based EMSs have been widely used in the marine industry. Nonetheless, their performance is largely contingent on the researchers' knowledge and engineering experience. Rule-based systems encounter challenges in achieving the optimal control [10]. Global optimization EMSs are typically unsuitable for real-time control, as prior operation information is generally unattainable. Thus, the global optimization EMSs are usually employed to validate the control strategies [11]. Equivalent consumption minimization strategy (ECMS) is a real-time optimization-based algorithm. Yet, it is only focused on fuel consumption without considering the energy reserved for the future or degradation of energy sources [12]. Model predictive control (MPC) is capable for handling constrained multi-variable problems with system estimation features and has been extensively implemented in land-based or electric vehicle (EV) power management applications [13]. Nevertheless, marine power systems differ significantly due to frequent load fluctuations and abrupt disturbances originating from the oceanic environment. Shipboard power system has its own special features and requirements, and MPC is one of the most promising optimal control strategies for marine applications.

In [14], the researchers presented an MPC-based ship power management controller to coordinate sources and loads based on future demand dynamically. A shipboard centralized MPC is proposed to optimize the coordination of the energy storage and diesel gen-sets (DGs) [15]. Hou et al. [16] designed pre-filtering MPC and coordinated control MPC method for ship power system to address the power flow tracking between super-capacitors and battery devices, and at the same time to achieve energy saving under various operating constraints. In [17], the MPC algorithm is combined with particle swarm optimization (PSO) control for the ship power management to achieve power-sharing between different power sources and maintain the DC voltage stability. An adaptive MPC algorithm was developed in [18] to handle the marine load fluctuations, improve system efficiency and reduce mechanical wear and tear. A financial model has been proposed to minimize the system operation cost, including hydrogen fuel cost and the cold-ironing cost [19], [20].

The main benefit of the MPC approach lies in its capacity to optimize the present time slot while also considering upcoming time slots. This inherent ability allows it to adapt well to highly dynamic systems. While MPC-based strategies are effective, most existing works only focus on one or two control criteria, aiming to enhance either system efficiency or dynamic performances. However, there is a gap in the field for a multi-objective optimization EMS, one that addresses not only dynamic power supply but also optimal fuel efficiency, emissions reduction, and overall power device preservation. Moreover, in real-time implementation, ensuring robust control performance amidst frequent load fluctuations and sudden disturbances poses a significant challenge.

In this paper, an adaptive model predictive control (AMPC)-based approach has been proposed to achieve multi-objective energy management control. Compared to existing studies on hybrid shipboard EMS control, the main contributions of this paper are as follows:

- An improved real-time EMS based on AMPC is proposed to provide an optimal power allocation between different power sources of the hybrid shipboard power plant to achieve minimum costs and in a novel control architecture for marine systems.
- A prototyping EMS controller has been developed and deployed to a programmable logic controller (PLC) hardware, and verified with a hardware-in-the-loop (HIL)-based plant.
- A case study is conducted on a targeted tugboat to validate the robustness of the proposed EMS control performance using three typical operational shipload profiles with power fluctuations.
- The control performance is measured through economic benefits that incorporates not just fuel efficiency, but also emission limits and power devices lifetime. Prior researches have been more focused on a single control criteria. A cost study is performed and the total cost of ownership for 10 years of long-term vessel operation has been calculated and compared with traditional EMS approaches.

This paper is organized as follows: the hybrid shipboard power system model is built and the shipload profile is defined in Section II. The proposed AMPC-based optimal EMS is presented in Section III. The HIL verification tests and a cost comparison study are performed and analyzed in Section IV. Conclusions are finally drawn in Section V.

II. SHIPBOARD POWER SYSTEM PLANT MODEL

A. SHIPBOARD POWER SYSTEM CONFIGURATION

In this study, a DC-grid hybrid shipboard power system is configured and modeled to verify the proposed EMS control performance. The parameters of the power devices refer to

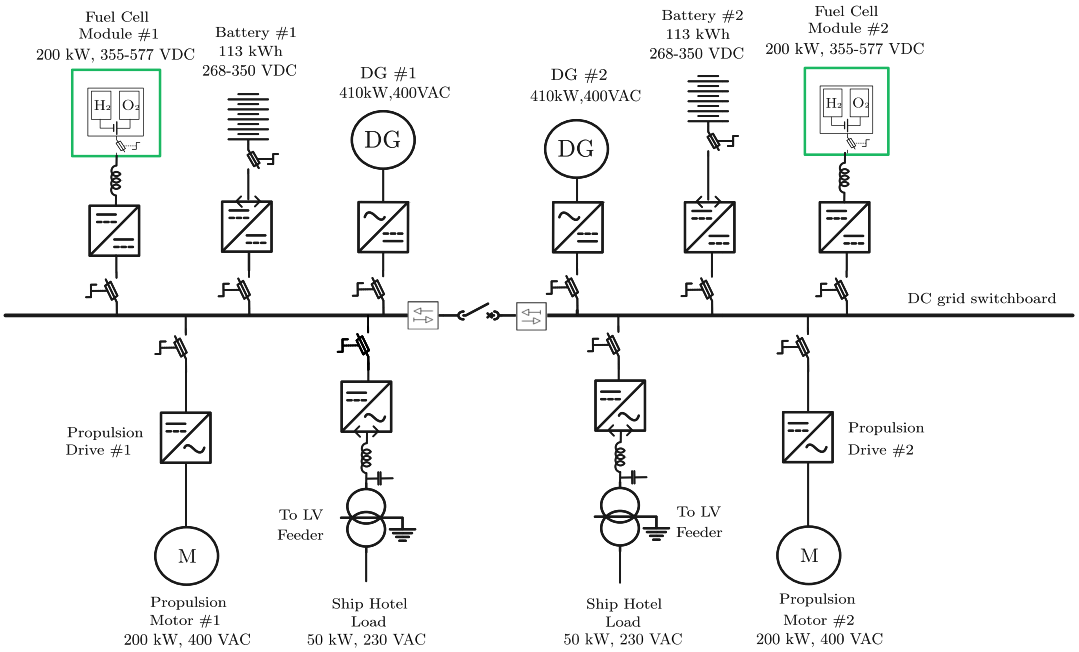

FIGURE 1. DC-distributed shipboard power system single line diagram.

those of tugboat from the Flagships project. The flagships is a commercial project of ABB, who provides the power and propulsion solution [21]. The demo shipboard power system configuration single line diagram is shown in Figure 1. Due to the marine special reconfigurability and redundancy requirements, this shipboard power plant comprises two sets of 200kW fuel cells, two battery arrays with capacity of 113 kWh each and two 410kW DGs as the back-up power sources.

This plant model operates on a HIL platform. The dynamic performance of each power system component is validated against a full-scale actual power plant facility presented in the authors' previous work [5].

B. HYBRID SHIPBOARD POWER SYSTEM MATHEMATICAL MODEL

The mathematical model of the demo shipboard power system is built in this section, which includes the fuel cells, batteries, and DGs as the power sources. The propulsion load and ship hotel loads of the vessel are represented with controllable current sources. The system model is given as follows.

1) Fuel cell model:
The proton-exchange membrane fuel cell (PEMFC) is the most mature technology over other types of fuel cell and is configured as the main power supply device in this study. The voltage of a PEMFC elementary cell can be written as follows [22]:

$$V_{cell} = E_{nernst} - V_{act} - V_{conc} - V_{ohm} \quad (1)$$

$$V_{fc} = N_{fc} \times V_{cell} \quad (2)$$

where V_{cell} is the voltage of a PEMFC elementary cell, E_{nernst} is the equilibrium voltage, V_{act} is the activation over-potential, V_{conc} is the concentration over-potential, V_{ohm} is the ohmic over-potential, V_{fc} is the voltage of PEMFC stack, and N_{fc} is the number of cells in series.

2) Diesel gen-set (DG) model:
DGs serve as the back up power in this demo system. The system consists of four main sections: fuel injection and diesel engine,synchronous generator (SG), governor, and automatic voltage regulator (AVR) [23]. The mathematical models of each part of DG are formed as follows:

- *Fuel injection and diesel engine* is presented by a time delay and the coupling shaft model, as in [24], [25]. The simplified model in s domain is given by

$$\frac{T_m(s)}{u_\omega(s)} = \frac{K_{en} \cdot e^{-t_d \cdot s}}{t_e s + 1} \quad (3)$$

$$J_{eq} \cdot \frac{d\omega_m}{dt} = T_m - T_e - k_{f_{eq}} \cdot \omega_m \quad (4)$$

where ω_m is the mechanical speed, u_ω is the control signal from the speed governor, T_m is the mechanical torque developed by the engine, J_{eq} is the equivalent inertia of the entire system, $k_{f_{eq}}$ is the equivalent friction coefficient, K_{en} is the engine gain, t_d is a delay representing the time elapsed from the fuel injection until the torque is developed at the engine shaft, and t_e is the time constant of the fuel injection.

- *Synchronous generator (SG)* is considered without damper windings for the sake of simplifying the

model. And its d-q rotating reference frame is given by

$$V_d = -r_s \cdot i_d + L_q \cdot \omega_e \cdot i_q + L_d \cdot \frac{di_d}{dt} + M_{sf} \cdot \frac{di_f}{dt} \tag{5}$$

$$V_q = -r_s \cdot i_q - L_d \cdot \omega_e \cdot i_d + L_q \cdot \frac{di_q}{dt} + M_{sf} \cdot \omega_e \cdot i_f \tag{6}$$

$$V_f = r_f \cdot i_f + L_f \cdot \frac{di_f}{dt} - M_{sf} \cdot \frac{di_d}{dt} \tag{7}$$

$$T_e = (L_d - L_q) \cdot i_d \cdot i_q + M_{sf} \cdot i_q \cdot i_f \tag{8}$$

where V_d, V_q, i_d, i_q are the output voltages and currents in the d-q rotating reference frame respectively, V_f and i_f are the field excitation voltage and current respectively, r_s and r_f are the stator winding and field winding internal resistances respectively, L_d and L_q are the stator inductance in the d-axis and q-axis respectively, L_f is the inductance of the field, M_{sf} is the mutual inductance between the field winding and the d-axis stator winding, and T_e is the electromagnetic torque.

- *Governor* is responsible for regulating the engine speed and maintaining the constant output frequency within the desired limits under different loading conditions. This governor also has the structure of a PI controller with the droop function implemented. This model can be given by

$$u_\omega = (\omega^*_{en} - \omega_{en} - k_{dr,freq} \cdot u_\omega)(K_{P_\omega} + \frac{K_{I_\omega}}{s}) \tag{9}$$

where K_{P_ω} and K_{I_ω} are the proportional and integral gains of the governor PI controller, and ω_{en} is the engine nominal speed and ω^*_{en} is the reference, and $k_{dr,freq}$ is the speed droop gain that equals $(m_{dr} \cdot \omega_{en})$, and m_{dr} is the static droop slope.

- *Automatic voltage regulator (AVR)* is to manage the terminal voltage (U_v) of the SG under different load conditions. This AVR is modeled as a first-order system, representing a power converter controlled by a PI controller [23], and is given by

$$V_f = \frac{k_{conv}}{t_{conv}s + 1} \cdot (U_v - k_{dr,v}V_f) \tag{10}$$

$$U_v = (K_{Pv} + \frac{K_{Iv}}{s}) \cdot (V^*_t - V_t) \tag{11}$$

where K_{Pv} and K_{Iv} are the proportional and integral gains of the AVR PI controller, k_{conv} and t_{conv} are the converter gain and time constant, and V^*_t and V_t are the reference and measured RMS output line voltage. $k_{dr,v}$ is the DC voltage droop rate for DC-distributed power system.

TABLE 1. Parameters for the DC-distributed demo vessel.

Fuel cell [26]	
Rated power ($P_{fc,i}$)	200 kW
Operating power range ($P_{fc,i\_min-max}$)	20-180 kW
Operating voltage ($V_{fc,i}$)	355-577 VDC
Rated current ($I_{fc,i}$)	514 A
Fuel cell efficiency ($\eta_{fc,i}$)	0.99
Fuel cell time constant ($\tau_{fc,i}$)	6.3 s
Fuel cell device cost (C_{fc})	USD 2100/kW
H_2 fuel cost (C_{H_2})	USD 12/kg
Diesel-genset [27]	
Rated power ($P_{gen,i}$)	410 kW
Nominal voltage (V_{abc})	400 VAC
Nominal current (I_{abc})	592 A
Genset efficiency ($\eta_{gen,i}$)	0.965
Genset time constant ($\tau_{gen,i}$)	3.31 s
410kW DG device cost (C_{gen})	USD 500,000
MDO fuel cost (C_{MDO})	USD 350/MT
GHG emission penalty (C_{GHG})	10% of C_{MDO}
Batteries [28]	
Capacity (Q_n)	113 kWh
Max. charge and discharge rate ($C_{batt,i}$)	2 C
Battery efficiency ($\eta_{batt,i}$)	0.98
Operating state of charge range ($SoC_{min-max}$)	10%-90%
Depth of Discharge (DoD)	0.8
Battery device cost (C_{batt})	USD 650/kWh
System-level parameters [21]	
Sample time (T_s)	0.1 s
DC-bus voltage (V_{dc})	580 VDC
Drive-train efficiency (η_{dt})	0.945
Drive-train time constant (τ_{dt})	0.26 s

3) Battery model:
Batteries are used to enhance the dynamic performance and shave the peak loads of the power system. The open circuit voltage (OCV) is defined distinctively for discharging and charging at a specified state-of-charge (SoC) due to the hysteresis effect [29]. The total voltage drop from OCV is then modeled here based on the first-order equivalent circuit to account for the internal resistance and polarization (OCV relaxation).

$$V_{term} = V_{OCV} - IR_e - V_p, \tag{12}$$

where V_{term} is the terminal voltage of the cell, V_{OCV} is the cell OCV, I is the current rate of the cell (positive for discharging and negative for charging), R_e is the electrical resistance (responsible for instantaneous voltage drop together with C_p, after the application of load) and V_p is the voltage drop across the polarization circuit. At any instant, V_p across the parallel RC circuit is represented by the voltage drop acrossR_p or C_p. So, the equation can be arranged by

$$\frac{V_p(t)}{R_p} + C_p \frac{dV_p(t)}{dt} = I(t) \tag{13}$$

where the total circuit current I of I_{Rp} and I_{Cp}, I_{Rp} is the current across polarization resistance, and I_{Cp} is the current across polarization capacitance.

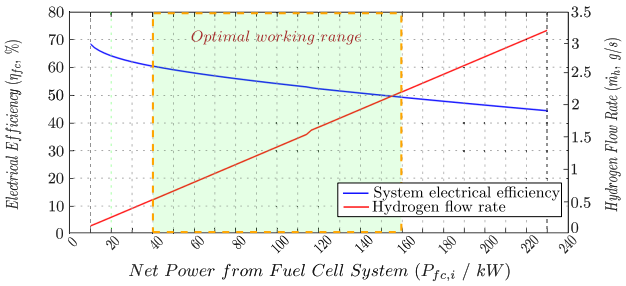

FIGURE 2. Simulated fuel cell system net efficiency and fuel flow rate.

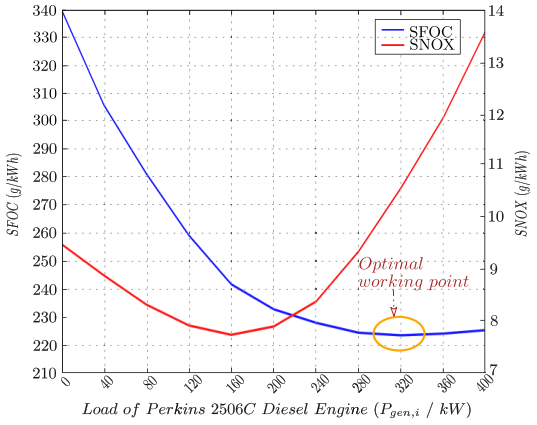

FIGURE 3. SFOC and SNOX of Perkins 2506C (410kW).

Transfer function after Laplace transform is as

$$V_p(s) = I(s)\frac{R_p}{1 + sR_pC_p} \tag{14}$$

So that the steady-state response of terminal voltage $V_{terms-s}$ to a given current is given by

$$V_{terms-s} = V_{OCV} - I(R_e + R_p) = V_{OCV} - IR_{ti} \tag{15}$$

where $R_{ti} = R_e + R_p$ is the total cell internal resistance. Battery SoC is intrinsically divided into two types: instantaneous SoC (SoC_{inst}) and nominal SoC (SoC_{nom}), both based on Ah counting. Nominal SoC is derived from nominal capacity based on standard discharging conditions as suggested by the manufacturer, while instantaneous SoC is based on the available instantaneous discharge capacity given by:

$$SoC_{nom}(t_i) = SoC_{nom}(t_{i-1}) - \frac{I_{step}(t_{i-1})t_{step}}{C_{nom}} \tag{16}$$

$$SoC_{inst}(t_i) = \frac{(1 - SoC_{nom}(t_{i-1}))C_{nom}}{C_{stepavail}(t_{i-1})} - \frac{I_{step}(t_{i-1})t_{step}}{C_{stepavail}(t_{i-1})} \tag{17}$$

where, I_{step} is the current at a given time step, t_{step} is the sampling time of battery management controller, and $C_{stepavail}$ is the capacity available for I_{step}. Instantaneous SoC is useful in indicating the capacity available at a given time step and operating conditions.

4) System Measurement:
The system model is capable of generating data for the fuel consumption, emissions and power device lifetime count.

- *Hydrogen (H_2) fuel consumption* during the operation period is given by

$$FC_{H_2} = \int_{t_0}^{t_f} \dot{m}_h(P_{fc,i})dt \tag{18}$$

where FC_{H_2} is the fuel consumption of hydrogen, t_0 and t_f are the beginning and the end time stamp of ship operation respectively. $\dot{m}_h$ is the specific device hydrogen flow rate (g/s) at loading condition of $P_{fc,i}$. The device efficiency and hydrogen flow rate are almost a linear function of the loaded power, as shown in Figure 2.

- *Marine diesel oil (MDO) fuel consumption* is totally different from the hydrogen fuel with fuel cell devices. As shown in Figure 3, the specific fuel consumption (sfc) for a marine diesel engine system can be written as:

$$sfc = \frac{\dot{m}_f}{P_B} \tag{19}$$

where $\dot{m}_f$ is the fuel flow rate in kg/s, and P_B is the ship engine brake power in W. The different prime movers usually have their own specific fuel oil consumption (SFOC) curve, which is referred to Perkins 2506C diesel engines in this study [27].

- *Green House Gas (GHG CO_2) emissions* are also taken into account, which is proportional to the fuel consumption. The quantity of GHG can be calculated by multiplying fuel consumption with fuel specific emission rate corresponding to the specific type of fuel used [30]:
  - Marine diesel oil (MDO): 3.206 tons of CO_2 per ton of oil consumed.
  - Heavy fuel oil (HFO): 3.114 tons of CO_2 per ton of oil consumed;
  - Light fuel oil (LFO): 3.151 tons of CO_2 per ton of oil consumed;

  In this study, the MDO fuel is selected if DG power is activated. To simplify the analysis, other emissions such as NO_x or SO_x are not taken into consideration.

The selected power system parameters and device costs for this demo vessel are shown in Table 1.

III. ADAPTIVE MODEL PREDICTIVE CONTROL (AMPC) FOR EMS

MPC algorithm is one of the most promising control methods for real-time shipboard power system applications. The classical MPC optimizer relies on a linear-time-invariant (LTI) dynamic model to predict system future behaviour (a relevant study can be found in the authors' previous work [31]). However, in actual practice, due to the nonlinear nature of shipboard power plant model and load fluctuations

in marine environment, LTI prediction accuracy is degraded. During the verification test, the HIL plant and communication protocol are introduced, the expected control performance becomes unacceptable. In order to ensure the efficacy of EMS and attain robust control, an adaptive model predictive control (AMPC) approach is proposed. This approach aims to develop a multi-objective EMS for the shipboard power system to minimize the overall TCO of vessel operation, including fuel consumption, emissions penalties, and power device degradation.

A. PROPOSED ADAPTIVE MPC-BASED EMS ARCHITECTURE

The AMPC approach solves the optimization problem over the prediction horizon by generating the control sequence at each time step. The number of elements in the control sequence is defined by the control horizon. And only the first components of the control decision sequence will be implemented in the power system. The prediction window moves to the next step and repeats the computation process [32]. The AMPC is proposed to make the controller insensitive to prediction errors and achieve robust control performance. AMPC addresses the degradation by adapting the prediction model for changing operating conditions, which allows the model parameters to evolve with time. In this study, Matlab/Model Predictive Control Toolbox software is implemented. At each control interval, the AMPC optimizer updates the plant model and nominal conditions. Once updated, the model and conditions remain constant over the prediction horizon.

A unique hierarchical supervisory control architecture is designed, as shown in Figure 4, which consists of a load prediction block, a linearized state-space system model, a mode selection module, and an AMPC-based real-time optimizer [32]. The load prediction block is to estimate the future power load ($\hat{P}_{load\_dmd}$), which is the pre-condition for the power and energy management control system design. The mode selection block designates the vessel operation mode and online power devices according to the predicted power load profile ($\hat{P}_{load\_dmd}$) and the system states (such as battery SoC_i). The selected operation mode ($\delta(k)$), the system state signals ($x(k)$) and the estimated state ($\hat{x}(k)$) are the input variables to the AMPC-based PMS optimization controller at time instant k. Optimal power allocation for different power sources ($u(k)$) is expected from the controller outputs. In addition, to verify the robustness of the proposed AMPC-based EMS algorithm, shipload power fluctuations ($d(k)$) are introduced according to the Sea State conditions.

B. POWER SYSTEM LOAD PROFILES

An accurate marine load prediction model is a prerequisite for the system to achieve optimal operation. A data-driven load prediction framework has been developed in authors' previous work [33]. However, due to the limited available operational data of the targeted tugboat needed for the

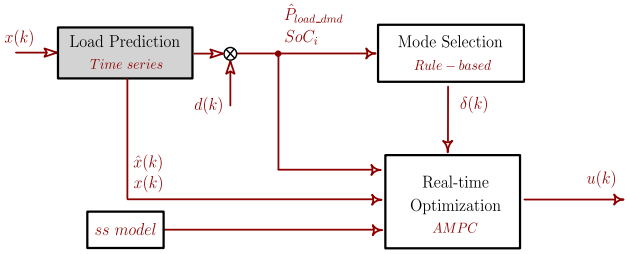

FIGURE 4. Hierarchical supervisory control architecture for proposed AMPC-based EMS.

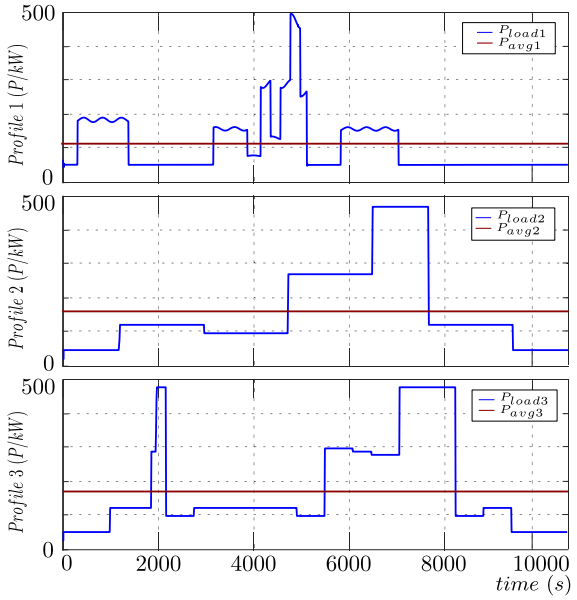

FIGURE 5. Pre-defined power load profile for demo vessel operation.

prediction, three typical tugboat load profiles are utilized in place of predicted load profiles, to verify the performance of the proposed EMS algorithm [30], [34], [35]. The shipload profiles (P_{load}) are shown in Figure 5. The tugboat operation can be categorized into three different working conditions: (1) *transit*, (2) *standby* or *idle*, and (3) *ship assist*. The tugboat starts to transit to the work location where the power load demand is around 30% of the total rated power onboard, followed by a standby period near the work location. And then, the tugboat enters the working zone for ship assisting operation, where peak load is required. When the assisting work is completed, the tugboat transits to the next work location or sails back to the harbor. The entire operating cycle is 3 hours (10800s) for this case study. The working process is similar, while variations exist in shipload demands and tasks. The average power load stands at about 10611 kW for Profile 1, 16810 kW for Profile 2, and 17880 kW for Profile 3.

Other shiploads, such as hotel or service loads, tend to be stable, usually exhibiting a consistent demand. In addition, the power requirements for the hotel and other onboard loads are typically minimal compared to the propulsion load, particularly for vessel types such as tugboats. Therefore, the impact of these other shiploads is not considered in this study.

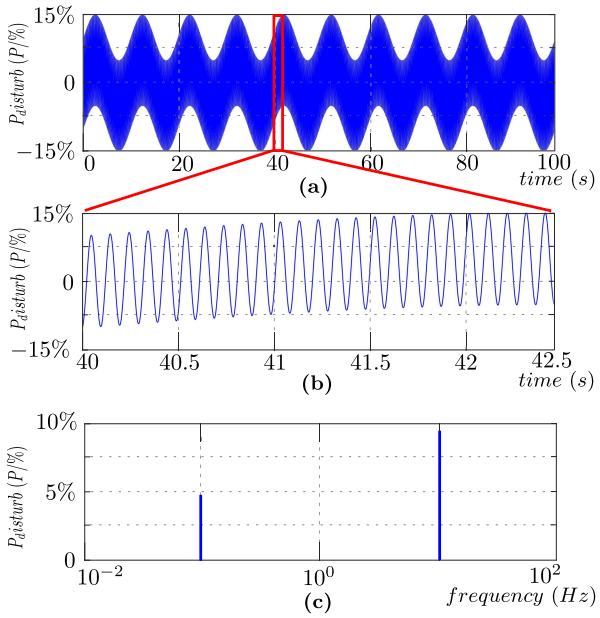

FIGURE 6. (a) Shipload power fluctuations, (b) zoom-in fluctuations, and (c) frequency spectrum.

C. SHIPLOAD FLUCTUATIONS

The shipload fluctuations and disturbances are the norm in the marine ocean environment, greatly impacting the control system performance. In this study, power load fluctuations ($d(k)$) are introduced into the shipload profile to evaluate further the effectiveness and robustness of the proposed power and energy management strategy.

The effects of fluctuations on the shipboard power plant largely depend on the motor control method. Different types of shipload fluctuations can be found in the literature [18]:

- Fluctuations from the impact of the first-order wave at the encounter-wave frequency;
- Fluctuation from the in-and-out-of-water effect;
- Fluctuations from propeller rotation at the propeller-blade frequency.

Shipload fluctuations and disturbances are complex mechanical-electric power conversion processes of ship dynamics [33]. The propeller characteristics, including thrust T_{prop}, torque Q_{prop} and power P_{load} are highly nonlinear function of motor shaft speed n_{prop}, water density ρ and propeller diameter D_{prop}, which can be given by [36]

$$\begin{aligned} T_{prop} &= sgn(n_{prop})\beta_{loss}\rho n_{prop}^2 D_{prop}^4 K_T \\ Q_{prop} &= sgn(n_{prop})\beta_{loss}\rho n_{prop}^2 D_{prop}^5 K_Q \\ P_{load} &= 2\pi n_{prop} Q_{prop} \end{aligned} \tag{20}$$

where K_T and K_Q are thrust and torque coefficients, which are defined by advance coefficient, pitch ratio, expanded blade-area ratio and number of blades. β_{loss} is the loss factor when the propeller goes in and out of the water.

In addition, the targeted demo tugboat usually operates along the coastal sea area and the sea state is considered calm. The World Meteorological Organization (WMO) Sea State 1 is used to estimate the amplitude of the disturbances for the targeted tugboat system [37]. In this study, to simplify the shipload fluctuation estimation, a 10Hz high-frequency power load is introduced, reflecting the rapid rotation of the propeller on the shaft. Additionally, a 0.1Hz low-frequency load is utilized to mimic the disturbances caused by ocean water wave movements [38]. The power disturbance parameters are selected according to Table 2. It is about 5% of the average power load for low-frequency disturbances and 10% of the average load for high-frequency fluctuations. Hence the total is about 15% disturbances of the average load power. The in-and-out-of-water fluctuation can be ignored due to the calm sea condition ($\beta_{loss} = 1$).

TABLE 2. Power disturbances parameters based on sea state I.

	Low frequency	High frequency	Total
Maximum power (Profile 1)	5kW	10 kW	15kW
Maximum power (Profile 2)	8kW	16 kW	24kW
Maximum power (Profile 3)	10kW	20 kW	30kW

The simulation results of the power fluctuations can be found for both the time and frequency domains in Figure 6. Large fluctuations are observed due to the propeller rotational motion and regular wave encounters.

D. STATE-SPACE MODEL

An LTI discrete-time, state-space (SS) model is needed for use as the basis for AMPC. The SS model can be given by

1) Fuel cell model:
The main power device fuel cell dynamics can be approximated as a first-order system in s-domain. The linearized model can be given by

$$P_{fc,i} = \eta_{fc,i} \cdot \frac{1}{\tau_{fc,i}s + 1} \cdot U_{fc,i} \tag{21}$$

where $P_{fc,i}$ is actual power drawn from the ith fuel cell. $U_{fc,i}$ is the power reference point of this specific fuel cell. $\eta_{fc,i}$ is the electrical efficiency and $\tau_{fc,i}$ is the fuel cell time constant according to the product data-sheet.

2) Diesel gen-set (DG) model:
DG dynamics is also presented by a first-order system:

$$P_{gen,i} = \eta_{gen,i} \cdot \frac{1}{\tau_{gen,i}s + 1} \cdot U_{gen,i} \tag{22}$$

where $P_{gen,i}$ is actual power drawn from the ith DG. $U_{gen,i}$ is the DG power reference. $\eta_{gen,i}$ is the electrical efficiency and $\tau_{gen,i}$ is the time constant of the DG.

3) Battery model:
The battery model is simplified and the SoC can be determined as [12]

$$\dot{SoC}_i = \frac{P_{batt,i}}{Q_n \cdot 3600} \tag{23}$$

where Q_n is the battery nominal capacity. $P_{batt,i}$ is the ith power output during charging ($P_{batt,i} > 0$) and discharging ($P_{batt,i} < 0$).

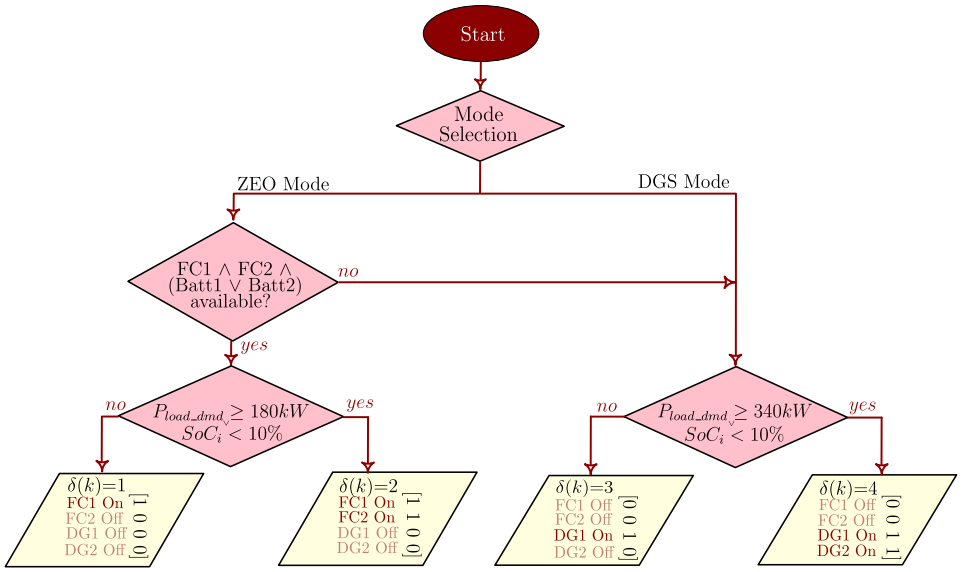

FIGURE 7. Rule-based Mode Selection Logic Flow Chart. Where ∧ is the AND logic, and ∨ is the OR logic.

4) Shipboard load model:
The total delivered power on the common DC bus from the shipboard power plant can be presented as [39]:

$$P_{supply} = \sum_{n=1}^{N_{fc}} P_{fc,i} + \sum_{n=1}^{N_{gen}} P_{gen,i} + \sum_{n=1}^{N_{batt}} \eta_{batt,i} \cdot P_{batt,i} \tag{24}$$

where P_{supply} is the sum of the power supply from all the power sources. $\eta_{batt,i}$ is the battery electrical efficiency. N_{fc}, N_{gen} and N_{batt} are the total number of the power devices, and they are 2 for each type.
The total delivered power is able to meet the load demand by considering the transmission losses and a tiny time delay [39]. The relationship between the load demand and supply can be given by

$$P_{load\_dmd} = \eta_{dt} \cdot \frac{1}{\tau_{dt} s + 1} \cdot P_{supply} \tag{25}$$

where P_{load_dmd} is the total load demanded power, η_{dt} is the drive-train efficiency for transmission losses, τ_{dt} is the drive-train time constant.

The entire hybrid power plant system state-space representation can be formed as follows:

$$\begin{aligned} x(k+1) &= Ax(k) + Bu(k) \\ y(k) &= Cx(k) \end{aligned} \tag{26}$$

with

$$x = \begin{bmatrix} P_{fc,1} \\ P_{fc,2} \\ SoC_1 \\ SoC_2 \\ V_{dc\_act} \\ P_{gen,1} \\ P_{gen,2} \\ P_{load\_dmd} \end{bmatrix}, \quad u = \begin{bmatrix} U_{fc,1} \\ U_{fc,2} \\ P_{batt,1} \\ P_{batt,2} \\ V_{dc\_ref} \\ U_{gen,1} \\ U_{gen,2} \end{bmatrix}, \quad y = x$$

where x is the state variables, u is the control variables, and y is the output variables. A, B, C, are the state matrices which represent the plant model. $P_{batt,i}$ is the power reference for battery systems. The DC voltage is to be defined by the power and energy management controller as V_{dc_ref}, and V_{dc_act} is the actual DC voltage feedback.

E. MODE SELECTION

Three different operation modes can be selected for this targeted vessel: zero emission mode (ZEO), hybrid mode (HYB), and pure diesel mode (DGS). In real application, DGs and fuel cells are not supposed to run in parallel under normal operation, and the HYB is only allowed in emergency cases. An example of such a case is when DGs are not able to produce full power. Therefore, the proposed optimal energy management control algorithm will be implemented and tested in ZEO and DGS mode only in this study.

For traditional EMS operation, the mode is determined by the vessel operator manually. With the improved optimized EMS strategy, the mode selection module is to define the vessel operation mode and the number of online power devices according to the shipload profile and the system states. Figure 7 shows the mode selection logic table. The selected mode ($\delta(k)$) and system state signals ($x(k)$) are the inputs to the AMPC controller at time instant k. Control variables ($u(k)$) are the generated power allocation commands for each power source. The power devices are to run only when it is necessary to. The objective of the mode selection module is to minimize the power device operating time so as to reduce the device degradation and the number of power equipment replacements during a long-term operation cycle.

ZEO is the default mode for normal vessel operation, which only enables the fuel cells and batteries as the power sources. Fuel cells are the main power supply, and the batteries support the load dynamics and peak load demand.

Due to the slow dynamic responses of fuel cell devices, the batteries need to be always online to absorb the load variations. In ZEO operation, the fuel cells are under power control mode, and the system DC voltage is determined by batteries. The primary fuel cell is always online, and the secondary fuel cell module will be switched on during peak load or when the battery SoC is below the safety margin(10% in this case study).

When the fuel cell device or hydrogen infrastructure is not available, the system will be switched to DGS mode. Similar to ZEO mode, the DGs are replacing the fuel cells to provide the main supply. The secondary DG will switch on during the peak load or low battery SoC. The primary DG terminal AC voltage determines the DC-bus voltage with a diode rectifier, and the batteries are under power control mode.

F. OPTIMIZATION EMS PROBLEM FORMULATION

The core of the AMPC optimizer is to define the cost function, which is formulated by a quadratic function that leads to minimizing the total cost of the multiple control objectives. It penalizes the deviation of the actual output from the reference input over the prediction horizon. The cost function for the proposed AMPC-based EMS is given by Equation 27, as shown at the bottom of the page.

N_p and N_c are the prediction and control horizon, $\alpha_1 - \alpha_8$ are the weighting factors for penalizing the control reference tracking errors while $\beta_1 - \beta_7$ are the weighting factors to compensate the sudden control action changes within the control horizon. P^*_{xx} are the optimal power reference of the particular power devices. For fuel cells, the system efficiency curve is almost a linear line and the optimal working range is between 20% to 80% of the total capacity. In this study, $P^*_{fc,i}$ is set at 50% ($100kW$) as the optimal reference point, as shown in Figure 2, to make sure that the fuel cells are always working within the optimal operating range. However, it is quite different for DGs. $P^*_{gen,i}$ are set at this most fuel-efficient point, about 75% of the diesel gen-sets total capacity, where SFOC is at the lowest in Figure3. Therefore, 300kW is selected as the optimal reference for DG in this case study. Since the *GHG* is proportional to the MDO consumption, it is also the optimal emission-efficient point. $\delta(k)$ is the operating mode, and there are two modes for selection: ZEO and DGS. $v(\delta(k))$ is the switch signal vector to control the power source equipment to be on or off, which means power reference to be placed either at the optimal set point (the power device is *ON*) or zero (the power device is *OFF*). For battery operation, SoC^*_i are set to the mid-range between the SoC limits (50%) to ensure the SoC of the battery is under the safe range without being over-charged or discharged. V^*_{dc} is set to 580 VDC as system DC-bus voltage. P_{load_dmd} is the actual power load profile to ensure that the load demand can be met.

G. SYSTEM CONSTRAINTS

- Power balance constraint: The total power supply and demand shall be balanced, which has been defined in Equation 24.
- Power source loading constraints:

$$\begin{aligned} P_{fc,i\_min} &< P_{fc,i} < P_{fc,i\_max} \\ P_{batt,i\_min} &< P_{batt,i} < P_{batt,i\_max} \\ P_{gen,i\_min} &< P_{gen,i} < P_{gen,i\_max} \\ SoC_{i\_min} &< SoC_i < SoC_{i\_max} \end{aligned} \tag{28}$$

$$\begin{aligned} min\ J = \sum_{j=1}^{N_p} \{ &+\alpha_1[P^*_{fc,1}(k+j)v(\delta(k))(1) - P_{fc,1}(k+j)]^2 + \alpha_2[P^*_{fc,2}(k+j)v(\delta(k))(2) - P_{fc,2}(k+j)]^2 \\ &+ \alpha_3[SoC^*_1(k+j) - SoC_1(k+j)]^2 + \alpha_4[SoC^*_2(k+j) - SoC_2(k+j)]^2 \\ &+ \alpha_5[V^*_{dc}(k+j) - V_{dc}(k+j)]^2 + \alpha_6[P^*_{gen,1}(k+j)v(\delta(k))(3) - P_{gen,1}(k+j)]^2 \\ &+ \alpha_7[P^*_{gen,2}(k+j)v(\delta(k))(4) - P_{gen,2}(k+j)]^2 + \alpha_8[P^*_{load\_dmd}(k+j) - P_{load\_dmd}(k+j)]^2 \} \\ &+ \sum_{j=1}^{N_c} \{ \beta_1[\Delta U_{fc,1}]^2 + \beta_2[\Delta U_{fc,2}]^2 + \beta_3[\Delta P_{batt,1}]^2 + \beta_4[\Delta P_{batt,2}]^2 \\ &+ \beta_5[\Delta V_{dc\_ref}]^2 + \beta_6[\Delta U_{gen,1}]^2 + \beta_7[\Delta U_{gen,2}]^2 \} \end{aligned} \tag{27}$$

with

$$\delta(k) = \begin{cases} 1 & ZEO\ (P_{load\_dmd} < 180\ kW\ \text{AND}\ SoC_i \geq 10\%) \\ 2 & ZEO\ (P_{load\_dmd} \geq 180\ kW\ \text{OR}\ SoC_i < 10\%) \\ 3 & DGS\ (P_{load\_dmd} < 340\ kW\ \text{AND}\ SoC_i \geq 10\%) \\ 4 & DGS\ (P_{load\_dmd} \geq 340\ kW\ \text{OR}\ SoC_i < 10\%) \end{cases}$$

$$v(\delta(k)) = \begin{cases} [1\ 0\ 0\ 0] & if\ \delta(k) = 1 \\ [1\ 1\ 0\ 0] & if\ \delta(k) = 2 \\ [0\ 0\ 1\ 0] & if\ \delta(k) = 3 \\ [0\ 0\ 1\ 1] & if\ \delta(k) = 4 \end{cases}$$

where for the 200kW fuel cell device used in this study, the power operating range is between 20kW to 180 kW. The maximum charging and discharging rate of the batteries are defined as 2C so that the operating range will be from -226 kW to 226 kW, and the batteries SoC is from 10-90%. The generator capacity is up to 410kW.

- Power source ramp rate constraints:

$$\frac{|P_{fc,i}(k+1) - P_{fc,i}(k)|}{\Delta t_{ramp}} < R_{fc,i\_max}$$
$$\frac{|P_{gen,i}(k+1) - P_{gen,i}(k)|}{\Delta t_{ramp}} < R_{gen,i\_max} \quad (29)$$

where R_{fc,i_max} and R_{gen,i_max} are the maximum rate of change in power of fuel cell and DG devices, respectively. Δt_{ramp} is the ramp time for energy source devices. The ramp limit is set to 10kW/s for fuel cells and 20kW/s for DGs according to the devices data-sheets.

IV. HARDWARE-IN-THE-LOOP VERIFICATION WITH IMPROVED AMPC-BASED EMS CONTROLLER

The proposed EMS controller is prototyped and its performance is tested with a HIL setup in the lab environment.

A. HIL TESTBED SETUP AND EMS CONTROLLER PROTOTYPING

Control system tests can be expensive, time-consuming and even potentially unsafe if it is used with an actual hardware plant. Therefore, a software-based plant model is considered to replace the actual system and different working conditions. In this study, a HIL setup has been built to verify the proposed control system behaviour, which can provide real-time hybrid shipboard power system responses, and also connect the controller and the system plant model with a real communication protocol. HIL testing is to ensure the high quality of control software by simulating the entire real-time hardware environment.

In this study, the hybrid shipboard power system mathematical model has already been introduced in Section II. The developed system plant model is built and runs on the Speedgoat target machine, which provides real-time dynamics of the shipboard power plant as well as the Fieldbus communication interface. The prototyped AMPC-based EMS controller is developed, converted to C language and then deployed to a programmable logic controller (PLC)-based embedded hardware. The B&R brand PLC X20CP3586 is used for this case study. The topology diagram for this HIL setup is shown in Figure 8. Profinet has been set up for this real-time testbed in the lab environment according to the actual industrial Fieldbus standard, as shown in Figure 9.

Speedgoat target machine is equipped with a powerful FPGA that can provide high-bandwidth and ultra-low latency. However, the HIL plant response rate is limited by the PLC cyclic time and the communication protocol transmission bandwidth. In real vessel operation, it is not necessary to set the PLC cyclic task time too small, since it is pointless to send

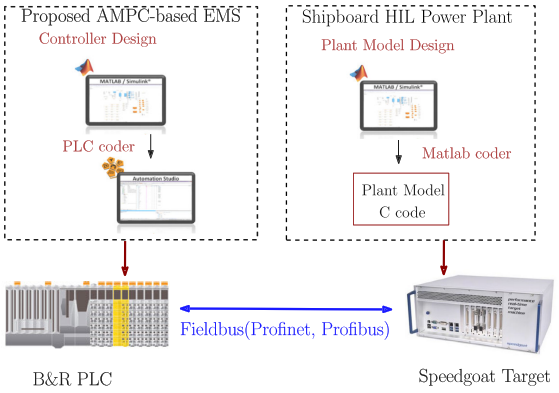

FIGURE 8. HIL topology scheme.

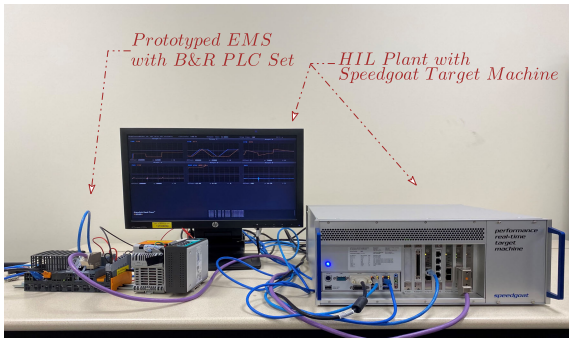

FIGURE 9. HIL setup in lab environment.

the commands faster than the power devices can respond. In this study, the PLC cyclic time is set to 100 ms, which is in line with the actual marine power control requirements.

B. RULE-BASED EMS TESTING RESULTS

The rule-based energy management algorithm is reliable, simple and cheap. Therefore, it has been implemented in the real marine vessel for decades. In this study, a rule-based EMS is tested as a benchmark with three different shipload profiles under two operating modes (ZEO and DGS). The verification testing results can be found in Figure 10 to Figure 12 for three shipload profiles respectively.

In ZEO mode, the fuel cells are selected as the main power sources, while the batteries are to support the dynamic response and shave the peak load. Both of the fuel cell modules are online in parallel regardless of the shipload demands or system states. Rule-based EMS controller is only to limit the loading and ramp limits of the fuel cell device according to the product data-sheet provided by the supplier. The battery system is to supply the rest of the power demands to fulfill the total shipload profile.

In DGS mode, the diesel gen-sets are switched on according to load demand. When the primary DG is loaded above the threshold line (85%), the secondary DG will be started up to support the peak load; when the average loading is below the stopping threshold (15%) of the total capacity, the secondary DG will stop and go offline.

It worth noting that battery systems are mainly discharged to provide peak load demand and enhance the system dynamics. With the shipload Profile 1, the peak load demand reach up to 500kW, but it does not last for too long and the battery initial SoC can be started from 50%. For Profile 2 and 3, more stored battery energy has been consumed due to the long peak loading period. A higher initial SoC is required to ensure the battery system is working under the safe operating range (10-90%). The initial SoC for Profile 2 and 3 cannot be too low (70% is set for the case study) to complete the entire tests.

C. CLASSICAL MPC-BASED EMS VERIFICATION TEST RESULTS

Classical MPC-based EMS strategy is also implemented [31], which is used to compare with the proposed improved AMPC strategy. The problem formulation is similar as the proposed AMPC, which uses a linear-time-invariant (LTI) dynamic model to predict future system behaviour. However, the SS model input is not required to specify the prediction model when computing the optimal plant manipulated variables. Due to the sensitivity to the prediction errors, the classical MPC is only performed in Matlab/Simulink environment. The simulation results for MPC-based EMS are shown in Figure 13 to 15 for all the three shipload profiles.

In ZEO mode, the primary fuel cell supports the power demand throughout the vessel operation. The secondary fuel cell is only online during the peak load, or the battery SoC is under the safety margin. With the great help of battery systems, the power output of the primary fuel cell is flattened regardless of the load variation, which improves the system stability and is beneficial to device lifetime extension.

In DGS mode, only one main DG is needed to meet the load demand together with the battery banks for all three shipload profiles. The power drawn from the DG system is smoothed. Battery sources are here to enhance the system dynamics and shave the peak load.

Furthermore, the shipload profiles have their patterns and the average load is also at different power levels, therefore it is difficult to use one common MPC controller to handle different ship operating tasks. Usually the operating mode and vessel work conditions are requested by the ship operator. The corresponding EMS controller will be enabled for implementation. Six EMS controllers are needed in this case study, with 3 shipload profiles and 2 working modes to fulfill the multiple ship operation tasks. The weights for the proposed MPC-based EMS controllers are shown in Table 3.

In summary, the dynamic responses of the shipboard power system have been greatly improved than rule-based approach. The power output from the main power sources is smooth and stable. The stability of the entire system has been strengthened. The average power is tracking closer to the optimal working point, and energy efficiency in improved. The total operation time has been cut down for fuel cell devices, and the huge device replacement cost is expected to be reduced. The battery SoC for different profiles is able to adjust automatically within a safe operating range. The TCO of the vessel operation can be reduced with the proposed MPC-based EMS control. The classical MPC approach lays the foundation for further improvement and development. A more detailed cost study will be presented in Section IV-E.

TABLE 3. Proposed MPC-based EMS weight factors for three profiles under two operating modes.

	Profile 1		Profile 2		Profile 3	
	ZEO	DGS	ZEO	DGS	ZEO	DGS
α_1	2	8	1.5	8	2.2	8
α_2	2.8	8	1.2	8	1.8	8
α_3	4e6	4e6	4e6	4e6	4e6	4e6
α_4	4e6	4e6	4e6	4e6	4e6	4e6
α_5	0.45	0.45	0.45	0.45	0.45	0.45
α_6	10	0.3	10	0.35	10	0.25
α_7	10	8	10	8	10	8
α_8	20	20	20	20	20	20
β_1	12	0.5	2	0.5	2	0.5
β_2	12	0.5	12	0.5	12	0.5
β_3	0.002	0.005	0.002	0.001	0.002	0.001
β_4	0.002	0.005	0.002	0.001	0.002	0.001
β_5	0.15	0.58	0.15	0.3	0.15	0.25
β_6	0.58	0.58	0.58	0.3	0.58	0.25
β_7	0.35	0.35	0.35	0.35	0.35	0.35

D. AMPC-BASED EMS WITH DISTURBANCES VERIFICATION TEST RESULTS

In order to demonstrate the further improvement and robustness of the proposed AMPC-based EMS, verification tests have been performed against the HIL plant with the shipload power fluctuations, which has been discussed in Section III-C. The verification test results are shown in Figure 16 to Figure 18 for the three shipload profiles.

In ZEO mode, the primary fuel cell maintains a stable power output with limited load variation. The secondary fuel cell is only online during the peak load or when battery SoC is at a low level. The battery systems support the peak demands and absorb most of the shipload fluctuations. The proposed AMPC-based EMS helps to improve the system stability and reduce the fuel cell device operating time.

In DGS mode, only one DG is needed to fulfill the entire three profiles' shiploads. The DG output power is smooth and no DG startup or shutdown operation is required. The batteries function as the energy buffer to enhance the system dynamics and peak loading capability. Majority of the shipload fluctuations are absorbed by battery systems.

The weight factors tuning is key for AMPC-based EMS controller design. However, the tuning process is complicated and time consuming. For different shipload profiles and operating modes, the weightage might be different. Usually, a heavy weightage is assigned to the variables that are required to have better tracking performance. In this study, the power load demand (α_8) needs to have a heavy weight to balance the power flow between supply and demand. The weight factors for battery SoC reference (α_3 and α_4) are multiplied by a factor of 10^6, so that SOC value (between

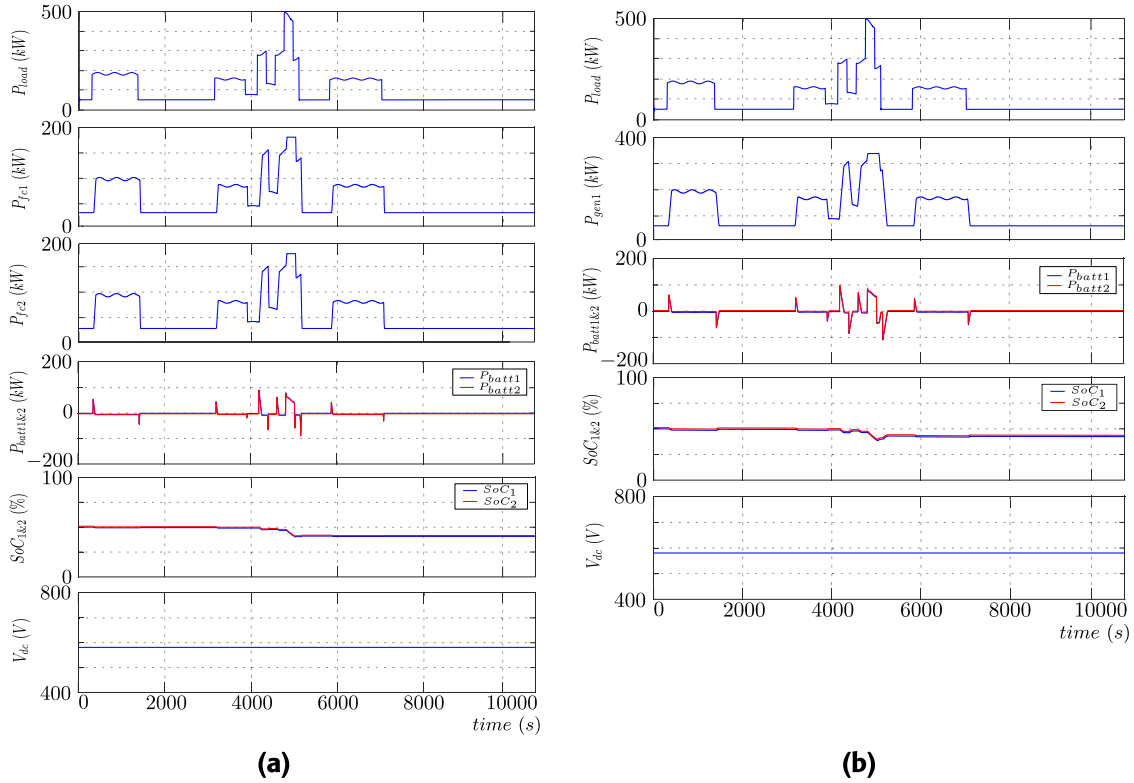

FIGURE 10. Rule-based EMS simulation test for hybrid shipboard demo vessel with load Profile 1: (a) ZEO mode; and (b) DGS mode.

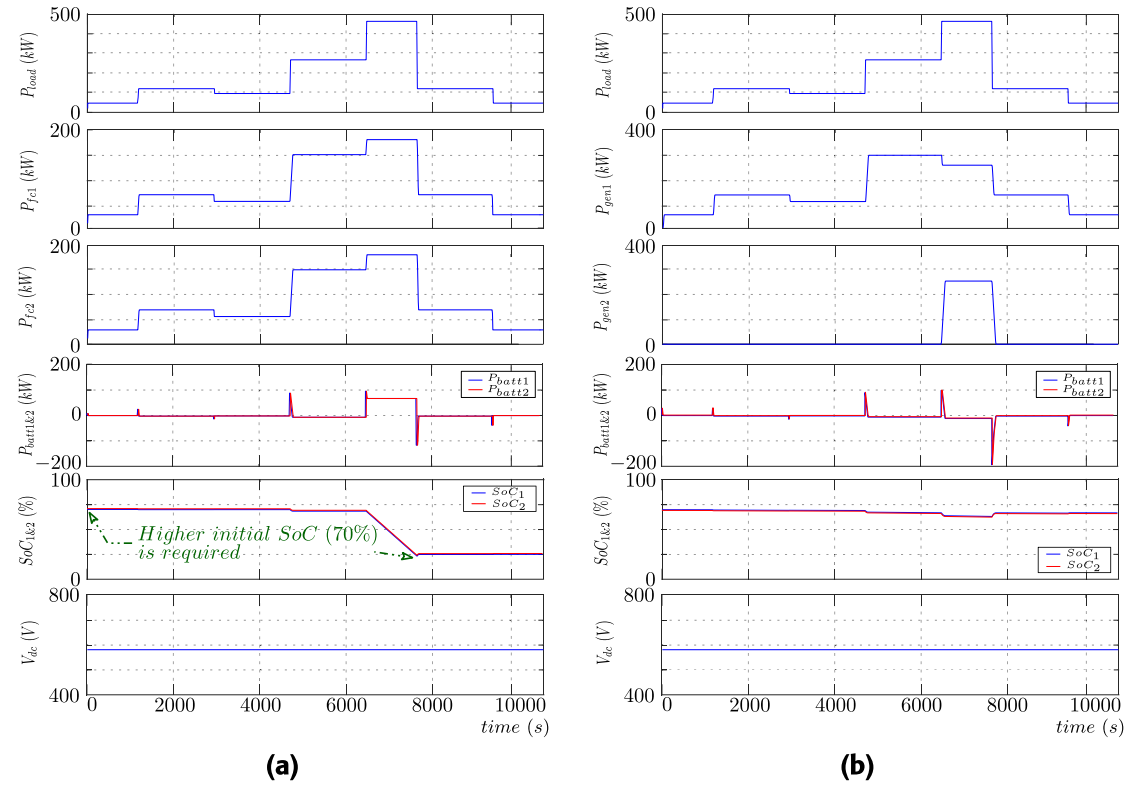

FIGURE 11. Rule-based EMS simulation test for hybrid shipboard demo vessel with load Profile 2: (a) ZEO mode; and (b) DGS mode.

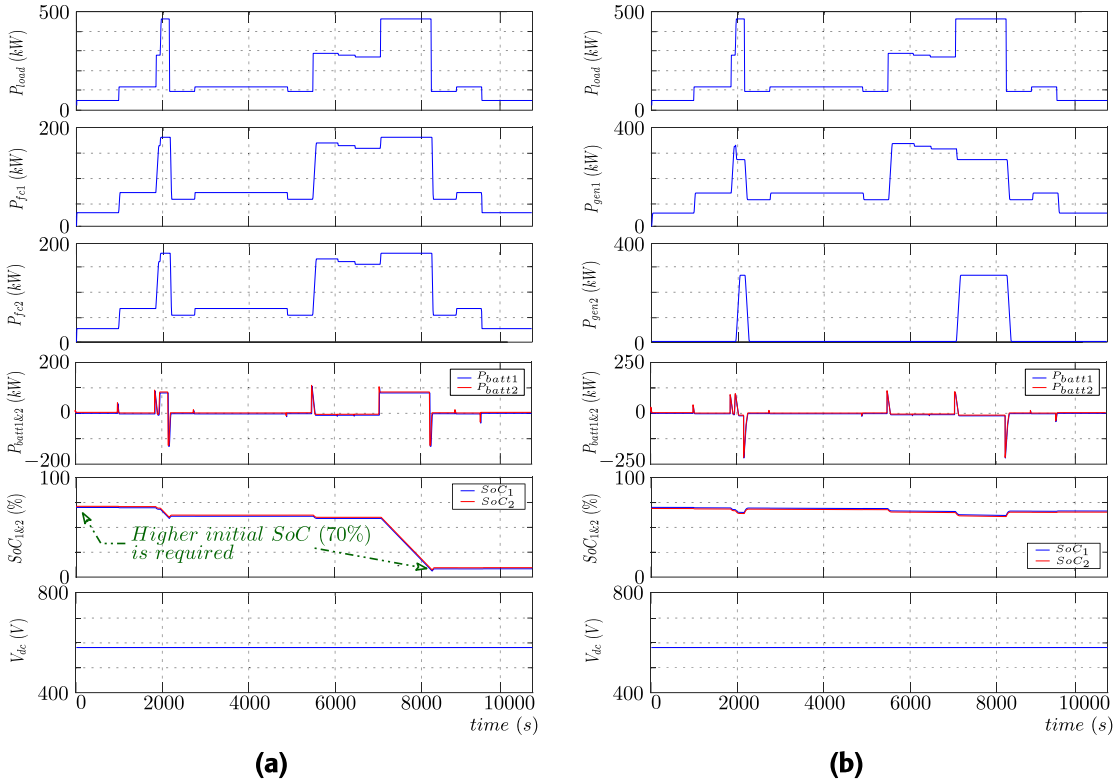

FIGURE 12. Rule-based EMS simulation test for hybrid shipboard demo vessel with load Profile 3: (a) ZEO mode; and (b) DGS mode.

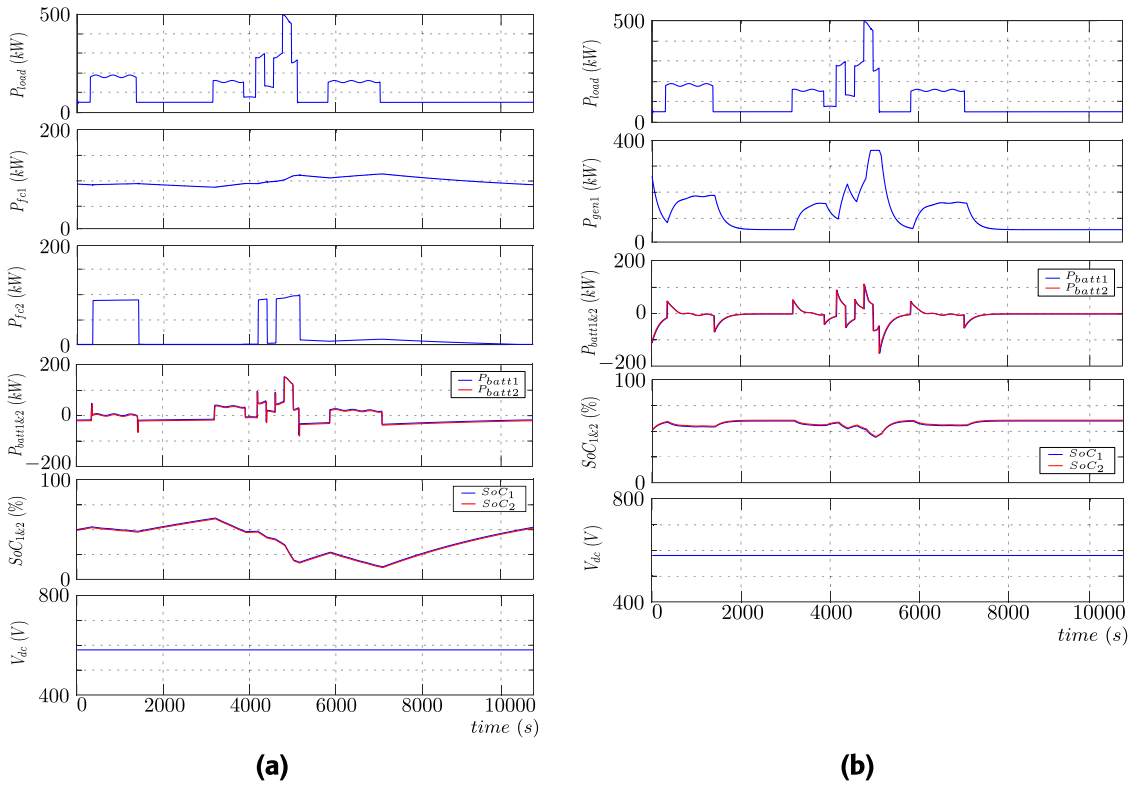

FIGURE 13. Classical MPC-based EMS Simulation test for hybrid shipboard demo vessel with load Profile 1: (a) ZEO mode; and (b) DGS mode.

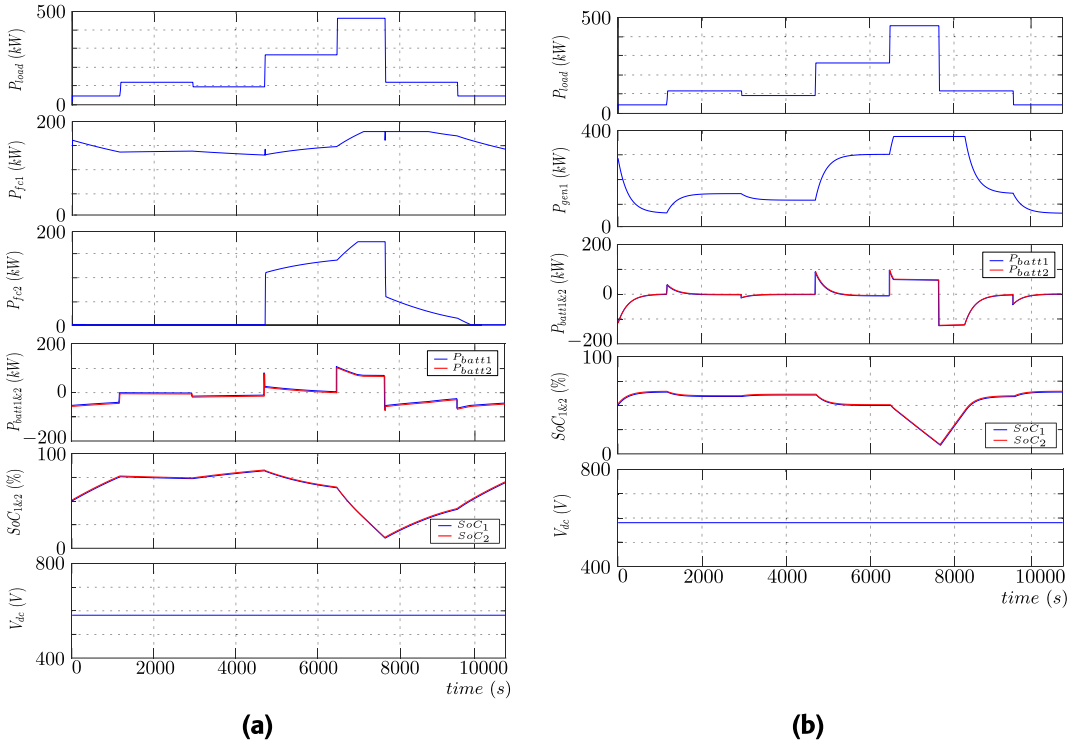

FIGURE 14. Classical MPC-based EMS simulation test for hybrid shipboard demo vessel with load Profile 2: (a) ZEO mode; and (b) DGS mode.

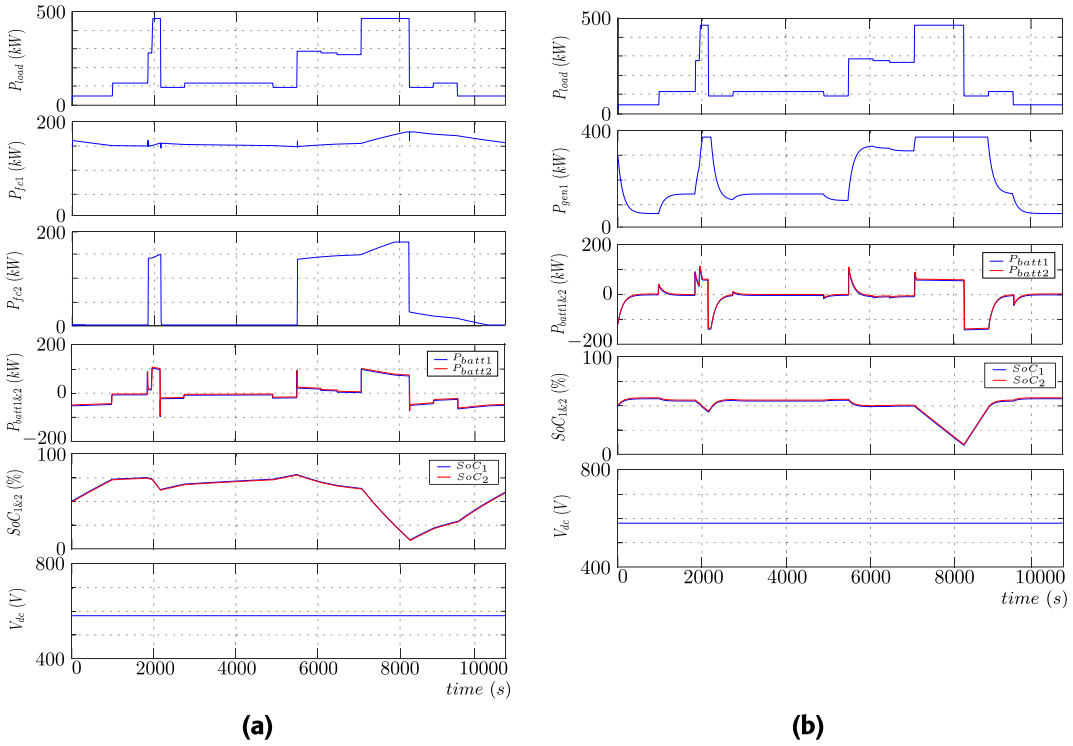

FIGURE 15. Classical MPC-based EMS simulation test for hybrid shipboard demo vessel with load Profile 3: (a) ZEO mode; and (b) DGS mode.

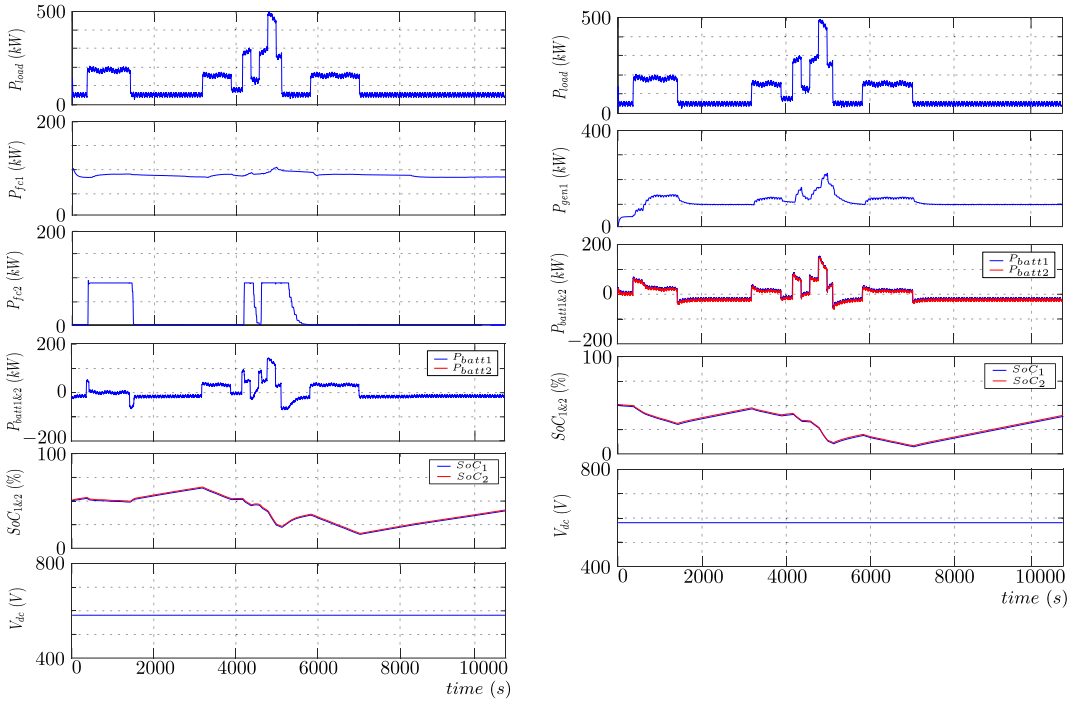

FIGURE 16. AMPC-based EMS HIL verification test for hybrid shipboard demo vessel with disturbances for load Profile 1: (a) ZEO mode; and (b) DGS mode.

TABLE 4. Proposed AMPC-based EMS weight factors for three profiles under two operating modes.

	Profile 1		Profile 2 & 3	
	ZEO	DGS	ZEO	DGS
α_1	5	8	3	8
α_2	50	8	12	8
α_3	1e6	1e6	1e6	1e6
α_4	1e6	1e6	1e6	1e6
α_5	10	10	10	10
α_6	4	8	4	7.4
α_7	4	18	4	18
α_8	20	20	20	20
β_1	100	1	500	1
β_2	200	1	550	1
β_3	0.002	0.0001	0.0001	0.0001
β_4	0.002	0.0001	0.0001	0.0001
β_5	0.15	0.15	0.15	0.15
β_6	0.58	800	0.58	1100
β_7	0.35	100	0.35	600

0 to 1) can be of a similar order of magnitude as other state variables expressed for power (10^6 W). In addition, the weights to penalize the control actions for both the fuel cells and DGs (β_1 and β_2) are set to a relatively higher value to mitigate abrupt changes. Lower weighting factors are set for the battery power (β_3 and β_4), since batteries are to handle shipload power fluctuations with fast response time.

Similar to the classical MPC-based EMS strategies, multiple EMS controllers are needed to fulfill the different ship operation tasks. The weight factors for both ZEO and DGS mode are shown in Table 4.

It is worth noting that during the tuning process, shipload Profile 2 and 3 can share the same controller weight factors without any control feature losses. This means the AMPC-based EMS can handle both shipload Profiles 2 and 3 with the same controller. The reason is that these two working profile patterns are similar and the average power demand does not have many gaps (about 6.37% deviation). Therefore, the AMPC-based EMS is able to handle small load fluctuations and even different ship operating tasks as long as it is within the safety margin. Robust control is achieved, and only four controllers are required instead of six for this case study.

In addition, the AMPC-based EMS control also has the capability to adjust the battery SoC during the vessel operation. For both ZEO and DGS mode, the battery initial SoC for three profiles all start from 50%. While for the rule-based EMS, a valid initial SoC condition should be fulfilled to ensure the completion of the vessel operational cycle.

On the other hand, based on the testing results shown in Figure 13- 18, there is no necessity to activate the secondary power source under DGS mode operations. This is attributable to the fact that a single primary DG is sufficient to fulfill the power shipload profiles. Running both DG and FC simultaneously is not a typical procedure in vessel operations. This is also the reason that HYB mode is not required in EMS optimization operations.

Nevertheless, the model predictive control algorithm is not perfect. The computation cost is high due to the intensive

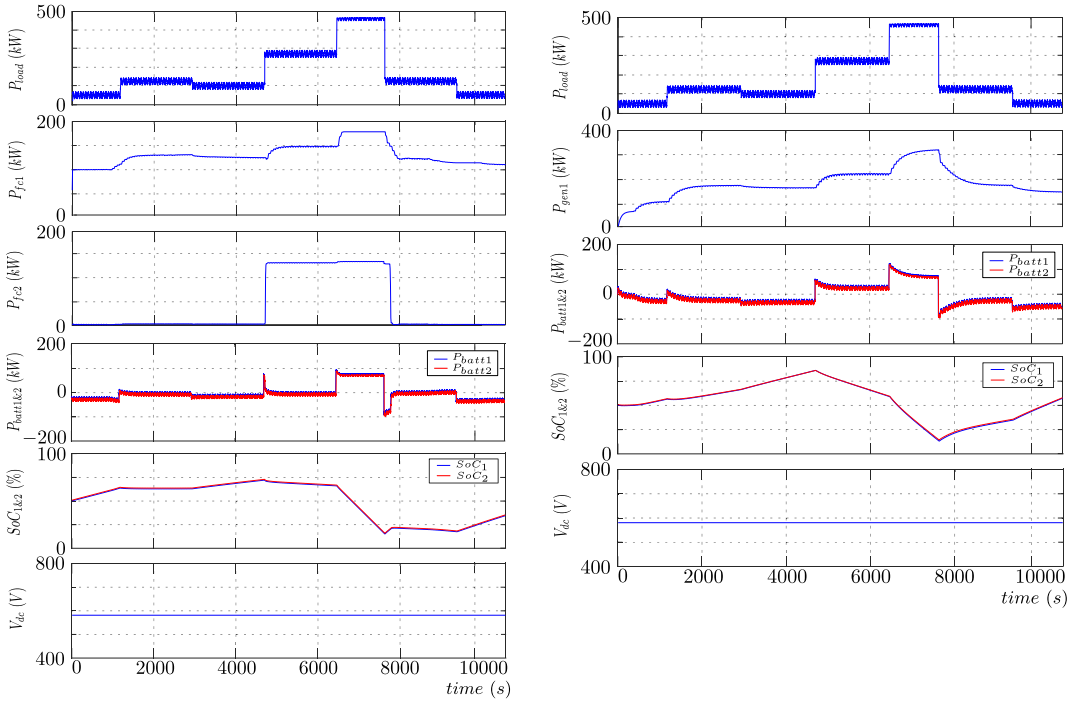

FIGURE 17. AMPC-based EMS HIL verification test for hybrid shipboard demo vessel with disturbances for load Profile 2: (a) ZEO mode; and (b) DGS mode.

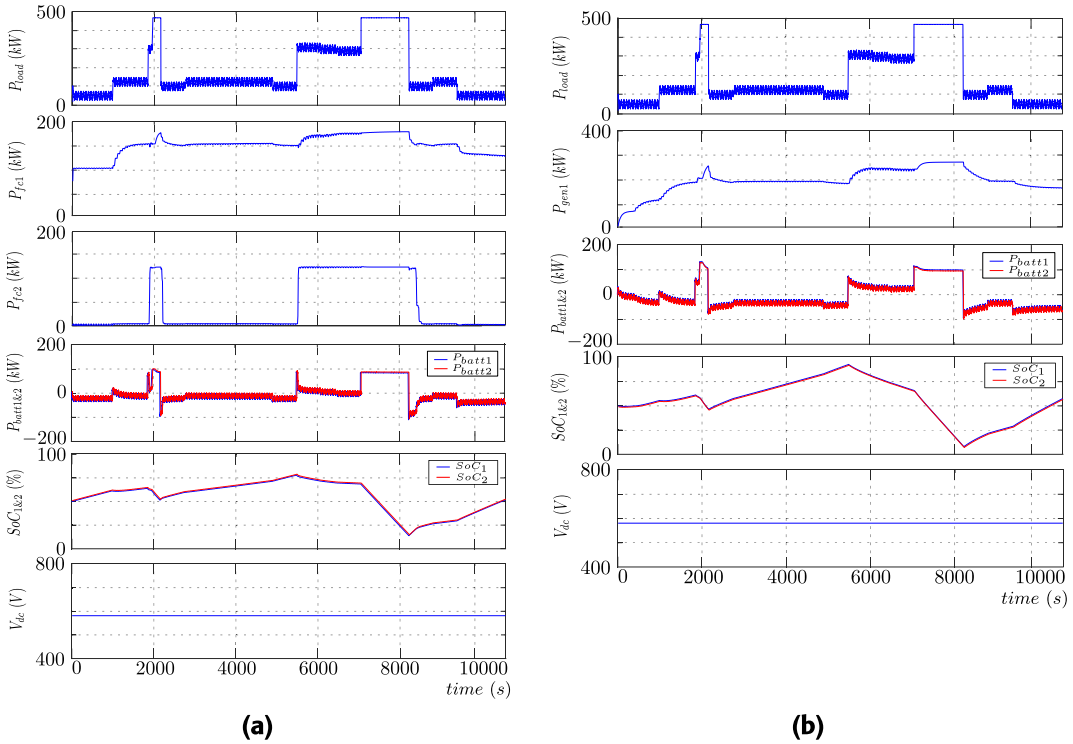

FIGURE 18. AMPC-based EMS HIL verification test for hybrid shipboard demo vessel with disturbances for load Profile 3: (a) ZEO mode; and (b) DGS mode.

calculations required. And the controller design is more complex and time-consuming. During the verification testing, the average CPU load of the selected B&R X20 series PLC can climb to 85%, which is considered a high level. On the other hand, the traditional rule-based method only requires an average CPU load of 27%. Hence, if the AMPC-based EMS

TABLE 5. Vessel operating comparison: ZEO mode.

	Profile 1			Profile 2			Profile 3		
	RB	MPC	AMPC	RB	MPC	AMPC	RB	MPC	AMPC
C_{H_2} (H_2 fuel cost)	$2,604,960	$2,682,720	$2,535,840	$4,462,440	$4,545,720	$4,331,280	$4,745,040	$5,150,160	$4,849,560
C_{fc} (Fuel cell device cost)	$1,260,000	$840,000	$840,000	$1,260,000	$840,000	$840,000	$1,260,000	$840,000	$840,000
C_{batt} (Battery device cost)	$146,900	$146,900	$146,900	$146,900	$220,350	$146,900	$146,900	$220,350	$220,350
C_{total} (Total cost: USD)	$4,011,860	$3,669,620	$3,522,740	$5,869,340	$5,606,070	$5,318,180	$6,151,940	$6,210,510	$5,909,910
Savings in total fuel cost	-	-2.99%	**2.65%**	-	-1.87%	**2.94%**	-	-8.54%	-2.20%
Savings in TCO	-	8.53%	**12.19%**	-	4.49%	**9.39%**	-	-0.95%	**3.93%**

TABLE 6. Vessel operating comparison: DGS mode.

	Profile 1			Profile 2			Profile 3		
	RB	MPC	AMPC	RB	MPC	AMPC	RB	MPC	AMPC
C_{MDO} (*MDO* fuel cost)	$384,090	$376,080	$369,642	$559,320	$577,560	$564,672	$600,240	$586,680	$580,440
C_{GHG} (*GHG* penalty)	$38,409	$37,608	$36,964	$55,932	$57,756	$56,467	$60,024	$58,668	$58,044
C_{batt} (Battery device cost)	$146,900	$146,900	$146,900	$146,900	$220,350	$220,350	$146,900	$220,350	$220,350
C_{gen} (DG device cost)	$500,000	$500,000	$500,000	$500,000	$500,000	$500,000	$500,000	$500,000	$500,000
C_{total} (Total cost: USD)	$1,069,399	$1,060,588	$1,053,506	$1,262,152	$1,355,666	$1,341,489	$1,307,164	$1,365,698	$1,358,834
Savings in total fuel cost	-	2.09%	**3.76%**	-	-3.26%	-0.96%	-	2.26%	**3.30%**
Savings in TCO	-	0.82%	**1.49%**	-	-7.41%	-6.29%	-	-4.48%	-3.95%

is adopted, a PLC with a greater calculation capacity might be necessary.

E. COST COMPARISON STUDIES

With the help of the AMPC-based EMS, the power drawn from the main source devices is smoothed. The load fluctuations and disturbances are mostly absorbed by the battery systems, and the main power devices are to provide the average shipload demands. Unlike the rule-based energy management control, there are no specific initial conditions required for the shipboard power system. The proposed AMPC-based EMS not only greatly improves the entire power network stability but is also beneficial to the device lifetime extension, especially for fuel cell systems.

In addition, during the verification tests for the three case study profiles, the total fuel consumption and power device usage hours are recorded. A 10 years of long-term TCO for vessel operation is calculated. It is assumed that there are 50 working weeks per year for the target vessel, and each week comprises 6 working days and 4 work task cycles per day, making up 36,000 operating hours in total for 10 years operation. The hydrogen fuel cost, MDO fuel cost, the emission penalty for MDO fuel, and the total power device capital cost are all considered. The TCO for both ZEO and DGS modes can be compared according to the Table 5 and 6.

In ZEO mode, hydrogen fuel cost remains the same level across all three EMS strategies. However, optimization-based EMS significantly reduces the operating hours of fuel cell devices. It eliminates the need for device replacement over a 10-year operating cycle (the fuel cell lifetime is about 25,000 hours [26]). In contrast, one device replacement is required for rule-based approach. And a considerable total cost reduction can be achieved. AMPC algorithm exhibits the highest performance among the three EMS strategies, which can achieve 12.19% TCO saving for Profile 1 operation, 9.39% and 3.93% cost reduction for Profile 2 and 3 respectively. With the current battery system size, it can support the Profile 1 operation for 14.85 years. This implies no device replacement is needed during the standard 10-years vessel operation cycle. However, the batteries can only last up to 9.85 years for Profile 2, and 9.09 years for Profile 3. One replacement is required for the batteries within the 10-years operation period. In real practice, the vessel will not only work for one ship operating task. Usually, it is a combination of the above three or even incorporate additional profiles. Therefore, there is huge potential to achieve higher TCO savings by avoiding battery replacements in actual vessel operations.

In DGS mode, it can be seen that one DG system is powerful enough to support the entire load demand according to the verification tests with the help of optimization-based method. There is no DG startup or shutdown operation, and the power output is smoothed by the energy storage battery devices. However, the fuel efficiency improvement is not significant, as is the TCO savings. The main reason is because the optimization-based algorithm heavily use the battery systems, which is a relatively more 'expensive' power source compared with MDO. Rule-based EMS control is a reliable and cost-effective control method for traditional MDO-fueled vessels and has been widely accepted by the marine market for decades. The main advantages with MPC and AMPC approaches for DGS mode operation mainly come from the system stability improvements and dynamic performances rather than the economic benefits.

V. CONCLUSION

In this paper, a supervisory optimization-based EMS has been proposed with an adaptive model predictive control approach, which is able to handle the load fluctuations and improve the system stability and minimize the TCO of vessel operation.

Compared with the traditional rule-based EMS control, the proposed AMPC algorithm is able to achieve savings of up to 12.19% of TCO and zero power device replacement through the 10 years of vessel operation cycle under ZEO mode.

The beauty of the proposed AMPC algorithm is the ability to balance the components of fuel consumption, emission and device usage as a whole to find a total minimum, and the TCO savings are significant. However, the cost reduction is not that evident under DGS mode. Although the AMPC-based EMS is able to reduce some MDO fuel cost and emissions penalty under some load profiles, battery devices are heavily used. Therefore, the overall savings in TCO is meagre. However, according to the latest class rules and regulations, a fairly high number of the existing fleet would need to undergo design or operational changes to improve their carbon intensity to reach the minimum compliance. It is possible to observe that up from 43% to 71% of the vessels would fall under categories D or E of the Carbon Intensity Index (CII) mechanism by 2026 [40]. Consequently, ship owners and shipbuilding industries must evaluate retrofits to improve ship maintenance and operations. The turning from MDO towards clean energy, such as hydrogen, becomes an inevitable movement to achieve lower carbon footprint. MDO-fueled vessels will slowly lose their dominant position and be completely replaced by other clean energy-fueled vessels eventually. Therefore, the proposed AMPC-based optimal EMS will become more critical and meaningful for actual practice in the near future.

The failure mode operation is not included in this study due to the page limitation. Future work to be done may include a comprehensive failure modes and effects analysis (FMEA) which encompasses consideration for fault tolerance and black-out recovery schemes during the emergency operation. In addition, in the pursuit of precise energy management control, an accurate shipload prediction has emerged as a prerequisite for system optimization. The authors have proposed a data-driven workflow to build a load prediction model for ship propulsion system [33]. Yet, the available data is still insufficient for effective load profile estimation training. Further studies are anticipated in vessel operational data collection and shipload profile prediction modelling. The predicted shipload profile can be derived from the prediction model, and then serve as the input reference to optimization-based EMS. The rolling-basis test should be engaged so that the 'living' load model can generate continuous profile data to mimic real-world ship operation scenarios.

REFERENCES

[1] *International Convention for the Prevention of Pollution From Ships*, Lloyd's Register, MARPOL, London, U.K., 2019.

[2] E. Hughes, "Initial IMO strategy on reduction of GHG emissions from ships," Int. Maritime Org., London, U.K., Tech. Rep. Resolution MEPC.304(72), 2018. [Online]. Available: https://wwwcdn.imo.org/localresources/en/KnowledgeCentre/IndexofIMOResolutions/MEPCDocuments/MEPC.304(72).pdf

[3] A. Haxhiu, A. Abdelhakim, S. Kanerva, and J. Bogen, "Electric power integration schemes of the hybrid fuel cells and batteries-fed marine vessels—An overview," *IEEE Trans. Transport. Electrific.*, vol. 8, no. 2, pp. 1885–1905, Jun. 2022.

[4] M. Al-Falahi, T. Tarasiuk, S. Jayasinghe, Z. Jin, H. Enshaei, and J. Guerrero, "AC ship microgrids: Control and power management optimization," *Energies*, vol. 11, no. 6, p. 1458, Jun. 2018.

[5] W. Chen, K. Tai, M. Lau, A. Abdelhakim, R. R. Chan, A. K. Ådnanes, and T. Tjahjowidodo, "DC-distributed power system modeling and hardware-in-the-loop (HIL) evaluation of fuel cell-powered marine vessel," *IEEE J. Emerg. Sel. Topics Ind. Electron.*, vol. 3, no. 3, pp. 797–808, Jul. 2022.

[6] Z. Zhang, C. Guan, and Z. Liu, "Real-time optimization energy management strategy for fuel cell hybrid ships considering power sources degradation," *IEEE Access*, vol. 8, pp. 87046–87059, 2020.

[7] P. Xie, J. M. Guerrero, S. Tan, N. Bazmohammadi, J. C. Vasquez, M. Mehrzadi, and Y. Al-Turki, "Optimization-based power and energy management system in shipboard microgrid: A review," *IEEE Syst. J.*, vol. 16, no. 1, pp. 578–590, Mar. 2022.

[8] S. B. Roslan, D. Konovessis, and Z. Y. Tay, "Sustainable hybrid marine power systems for power management optimisation: A review," *Energies*, vol. 15, no. 24, p. 9622, Dec. 2022.

[9] F. Mylonopoulos, H. Polinder, and A. Coraddu, "A comprehensive review of modeling and optimization methods for ship energy systems," *IEEE Access*, vol. 11, pp. 32697–32707, 2023.

[10] L. Meng, Q. Shafiee, G. F. Trecate, H. Karimi, D. Fulwani, X. Lu, and J. M. Guerrero, "Review on control of DC microgrids and multiple microgrid clusters," *IEEE J. Emerg. Sel. Topics Power Electron.*, vol. 5, no. 3, pp. 928–948, Sep. 2017.

[11] F. D. Kanellos, "Optimal power management with GHG emissions limitation in all-electric ship power systems comprising energy storage systems," *IEEE Trans. Power Syst.*, vol. 29, no. 1, pp. 330–339, Jan. 2014.

[12] L. W. Y. Chua, T. Tjahjowidodo, G. G. L. Seet, and R. Chan, "Implementation of optimization-based power management for all-electric hybrid vessels," *IEEE Access*, vol. 6, pp. 74339–74354, 2018.

[13] D. F. Pereira, F. D. C. Lopes, and E. H. Watanabe, "Nonlinear model predictive control for the energy management of fuel cell hybrid electric vehicles in real time," *IEEE Trans. Ind. Electron.*, vol. 68, no. 4, pp. 3213–3223, Apr. 2021.

[14] P. Stone, D. F. Opila, H. Park, J. Sun, S. Pekarek, R. DeCarlo, E. Westervelt, J. Brooks, and G. Seenumani, "Shipboard power management using constrained nonlinear model predictive control," in *Proc. IEEE Electr. Ship Technol. Symp. (ESTS)*, Jun. 2015, pp. 1–7.

[15] D. E. Gonsoulin, T. V. Vu, F. Diaz, H. Vahedi, D. Perkins, and C. S. Edrington, "Coordinating multiple energy storages using MPC for ship power systems," in *Proc. IEEE Electr. Ship Technol. Symp. (ESTS)*, Aug. 2017, pp. 551–556.

[16] J. Hou, J. Sun, and H. F. Hofmann, "Mitigating power fluctuations in electric ship propulsion with hybrid energy storage system: Design and analysis," *IEEE J. Ocean. Eng.*, vol. 43, no. 1, pp. 93–107, Jan. 2018.

[17] S. Paran, T. V. Vu, T. E. Mezyani, and C. S. Edrington, "MPC-based power management in the shipboard power system," in *Proc. IEEE Electr. Ship Technol. Symp. (ESTS)*, Jun. 2015, pp. 14–18.

[18] J. Hou, J. Sun, and H. Hofmann, "Adaptive model predictive control with propulsion load estimation and prediction for all-electric ship energy management," *Energy*, vol. 150, pp. 877–889, May 2018.

[19] M. Banaei, J. Boudjadar, T. Dragicevic, and M.-H. Khooban, "Cost effective operation of a hybrid zero-emission ferry ship," in *Proc. IEEE 11th Int. Symp. Power Electron. Distrib. Gener. Syst. (PEDG)*, Sep. 2020, pp. 23–28.

[20] M. Banaei, J. Boudjadar, and M.-H. Khooban, "Stochastic model predictive energy management in hybrid emission-free modern maritime vessels," *IEEE Trans. Ind. Informat.*, vol. 17, no. 8, pp. 5430–5440, Aug. 2021.

[21] Flagship. *Using River Power in River Boats Provides the Value Clean Waterborn Operation*. Accessed: Apr. 3, 2020. [Online]. Available: https://flagships.eu/2020/04/03/using-river-power-in-river-boatsproves-the-value-clean-waterborne-operations/

[22] M. M. Savrun and M. Inci, "Adaptive neuro-fuzzy inference system combined with genetic algorithm to improve power extraction capability in fuel cell applications," *J. Cleaner Prod.*, vol. 299, May 2021, Art. no. 126944.

[23] *IEEE Recommended Practice for Excitation System Models for Power System Stability Studies*, IEEE Standard 421.5-2016 (Revision IEEE Standard 421.5-2005), 2016.

[24] S. Roy, O. P. Malik, and G. S. Hope, "A low order computer model for adaptive speed control of diesel driven power-plants," in *Proc. Conf. Rec. IEEE Ind. Appl. Soc. Annu. Meeting*, Sep./Oct. 1991, pp. 1636–1642.

[25] M. A. Rahman, A. M. Osheiba, T. S. Radwan, and E. S. Abdin, "Modelling and controller design of an isolated diesel engine permanent magnet synchronous generator," *IEEE Trans. Energy Convers.*, vol. 11, no. 2, pp. 324–330, Jun. 1996.

[26] *PEM Fuel Cell Module for Heavy Duty Motive Applications—Product Data-Sheet*, Ballard, Burnaby, BC, Canada, 2018.
[27] *410 kW 2506 Data-Sheet*, Perkins, Memphis, TN, USA, 2012.
[28] *Corvus Orca Marine ESS (LG JP3 Cell) Data-Sheet*, Corvus Energy, Seattle, WA, USA, 2021.
[29] M. Farag, "Lithium-ion batteries: Modelling and state of charge estimation," M.S. thesis, Fac. Eng., McMaster Univ., Hamilton, On, Canada, Jun. 2013.
[30] L. C. W. Yuan, "Power management for all-electric hybrid marine power systems," Ph.D. dissertation, School Mech. Aerosp. Eng. (MAE), Nanyang Technol. Univ., Singapore, 2018.
[31] W. Chen, K. Tai, M. W. S. Lau, A. Abdelhakim, R. R. Chan, A. K. Ådnanes, and T. Tjahjowidodo, "Optimal power and energy management control for hybrid fuel cell-fed shipboard DC microgrid," *IEEE Trans. Intell. Transp. Syst.*, early access, Aug. 22, 2023, doi: 10.1109/TITS.2023.3303886.
[32] J. Kim, H. Kim, J. Bae, D. Kim, J. S. Eo, and K. K. Kim, "Economic nonlinear predictive control for real-time optimal energy management of parallel hybrid electric vehicles," *IEEE Access*, vol. 8, pp. 177896–177920, 2020.
[33] W. Chen, K. Tai, M. Lau, A. Abdelhakim, R. R. Chan, A. K. Ådnanes, and T. Tjahjowidodo, "Data-driven propulsion load profile prediction for all-electric ships," in *Proc. Int. Conf. Electr., Comput., Commun. Mechatronics Eng. (ICECCME)*, Nov. 2022, pp. 1–9.
[34] A. K. Birudula, A. K. Kesavarapu, T. R. Chelliah, D. Khare, and U. S. Ramesh, "Optimization with load prediction in asynchronous generator driven tugboat propulsion system," in *Proc. IEEE Transp. Electrific. Conf. (ITEC-India)*, Dec. 2017, pp. 1–6.
[35] T. L. Vu, J. S. Dhupia, A. A. Ayu, L. Kennedy, and A. K. Adnanes, "Optimal power management for electric tugboats with unknown load demand," in *Proc. Amer. Control Conf.*, Jun. 2014, pp. 1578–1583.
[36] M. M. Bernitsas, "KT, KQ and efficiency curves for the Wageningen B-series propellers," Univ. Michigan, Ann Arbor, MI, USA, Tech. Rep. 237, 1981. [Online]. Available: https://deepblue.lib.umich.edu/handle/2027.42/91702
[37] *National Meteorological Library and Archieve Fact Sheet 6—The Beaufort Scale*, Douglas Sea Scale, Nat. Meteorol. Library, Exeter, U.K., 2020.
[38] O. Faltinsen, *Sea Loads on Ships and Offshore Structures*. Cambridge, U.K.: Cambridge Univ. Press, 1990.
[39] L. Chua Wan Yuan, T. Tjahjowidodo, G. S. G. Lee, and R. Chan, "Optimizing fuel savings and power system reliability for all-electric hybrid vessels using model predictive control," in *Proc. IEEE Int. Conf. Adv. Intell. Mechatronics (AIM)*, Jul. 2017, pp. 1532–1537.
[40] *Zero Carbon Outlook—Setting the Course to Low Carbon Shipping*, ABS, Houston, TX, USA, 2022.

WENJIE CHEN (Member, IEEE) received the B.Sc. degree in automation from Shanghai Maritime University, Shanghai, China, in 2007, and the M.Sc. degree in electrical engineering from Ecole Polytechnique de l'Université de Nantes, France, in 2009. She is currently pursuing the joint Ph.D. degree in optimization control for power systems with Nanyang Technological University, Singapore, under the supervision of Prof K. Tai, and Katholieke Universiteit Leuven, Leuven, Belgium, under the supervision of Prof T. Tjahjowidodo. Then, she entered ABB, Singapore, as an Research Engineer. This research program is under the sponsorship of Singapore Economic Development Board and ABB Pte. Ltd.

KANG TAI received the B.Eng. degree in mechanical engineering from the National University of Singapore and the Ph.D. degree from the Imperial College London. He is currently an Associate Professor with the School of Mechanical and Aerospace Engineering, Nanyang Technological University, Singapore. His research interests include optimization, evolutionary computation, mathematical/empirical modeling of industrial processes, analysis of interdependencies, risks, and vulnerabilities in critical infrastructure networks.

MICHAEL WAI SHING LAU (Life Member, IEEE) received the Ph.D. degree. He is currently an Associate Professor with the Newcastle University in Singapore (NUiS). He is also a Control and Instrument Engineer with Defence and Oil and Gas Industry for about four years, before spending the next 35 years as an academia, first with NTU, until 2010, and is also with NUiS. His teaching and research interests include control, mechatronics system designs, and energy systems.

AHMED ABDELHAKIM (Senior Member, IEEE) was born in Egypt, in April 1990. He received the B.Sc. and M.Sc. degrees (Hons.) in electrical engineering from Alexandria University, Alexandria, Egypt, in 2011 and 2013, respectively, and the Ph.D. degree from the University of Padova, Vicenza, Italy, in 2019.

From August 2018 to May 2023, he was with ABB Corporate Research and held several positions as a Scientist, a Senior Scientist, and a Principal Scientist. He has been with Epiroc as the Global Electrification Program Manager, since June 2023. His research interests include power electronics converters and their applications for fuel cells and energy storage systems, investigation of new power converter topologies, and application of wide-bandgap (WBG) semiconductor devices (GaN/SiC) for high frequency and high-power density power converters.

Dr. Abdelhakim has received first classified excellent Ph.D. dissertation award from Societã Italiana di Electronica (SIE'19) among Italian universities, in 2019. He is also serving as an Associate Editor for IEEE TRANSACTIONS ON INDUSTRIAL ELECTRONICS.

RICKY R. CHAN received the Ph.D. degree in electrical engineering from Purdue University, USA, in 2009. He is currently the Research and Development Manager of ABB Marine & Ports, Helsinki, Finland, where he leads a team of specialists in the development of advanced electric solutions for marine applications.

ALF KÅRE ÅDNANES received the M.Sc. and Ph.D. degrees in electrical engineering from the Norwegian University of Science and Technology. He heads the Regional Division, AMEA of ABB Marine & Ports. He started with ABB, in 1991, and among previous positions in ABB, he was with Corporate Research and various positions within Marine, including delivery projects, engineering, in product management and development, and technology management with the Global Marine Business Unit, Marine & Ports.

TEGOEH TJAHJOWIDODO received the Ph.D. degree from KU Leuven, Belgium, in 2006. He has been an Associate Professor with the Department of Mechanical Engineering, KU Leuven, since 2019. From 2009 to 2019, he was with the School of Mechanical & Aerospace Engineering, NTU, Singapore, as an Associate Professor. He is involved in some projects related to his research interests include nonlinear dynamics, modeling, identification, and control, with a focus on monitoring for manufacturing.